NMR spectroscopy of some electrolyte solutions to 1.9 GPa

Gerardo Ochoa [a], Christopher A. Colla [b], Peter Klavins [c], Matthew P. Augustine [a,*],
William H. Casey [a,b,*]

[a] *Department of Chemistry, University of California, Davis, 1 Shields Ave, Davis, CA 95616, USA*
[b] *Department of Earth and Planetary Sciences, University of California, Davis, 1 Shields Ave, Davis, CA 95616, USA*
[c] *Department of Physics, University of California, Davis, 1 Shields Ave, Davis, CA 95616, USA*

Abstract

Nuclear-magnetic resonance (NMR) spectra of CsCl and LaCl$_3$ in D$_2$O/H$_2$O solutions were collected up to pressures of 1.9 GPa using a new NMR probe design that considerably extends the pressure range available for geochemical experiments. The longitudinal-relaxation times (T_1) for ^{2}H compare well with those reported in the previous studies of Lee et al. (1974), who examined lower pressures, and indicate that the probe functions properly. In some experiments, ^{133}Cs and ^{1}H NMR spectra could be taken on solutions to pressures well beyond the nominal freezing pressure of D$_2$O or H$_2$O to form Ice VI (near 0.9 GPa). Freezing to form the high-pressure ice is kinetically slow on an experimental time scale (minutes to hours). The data indicate that the electrolyte concentrations increase the freezing pressure of the solution. This result means that solution NMR spectra can be collected at pressures that are nearly twice the nominal freezing pressure of pure D$_2$O or H$_2$O. Pulsed-magnetic-field-gradient NMR methods are used to independently measure the self-diffusion coefficient of H$_2$O in these solutions, which yields estimates of solution viscosity via the Stokes–Einstein relation. The increased viscosity accounts for the pressure variation of T_1 values as rates of molecular tumbling are affected. Accounting for such changes is essential if NMR spectral line widths are used to infer pressure-enhanced rates of geochemical reactions, such as interconversion of aqueous complexes.
© 2016 Elsevier Ltd. All rights reserved.

Keywords: NMR; Aqueous geochemistry; High-pressure spectroscopy; Electrolyte solutions; Diffusion; Viscosity

1. INTRODUCTION

A common geochemical model of electrolyte solutions, the Helgeson-Kirkham-Flowers (HKF) model, describes the partial molar properties of solutes using an expression containing the dielectric constant of water and solute-specific variables derived from fits to experimental data. When this model is coupled to thermodynamic data for minerals, it can be used to estimate solubilities and speciation information at high pressures and temperatures (Shock and Helgeson, 1988; Tanger and Helgeson, 1988; Shock et al., 1989; Anderson and Crerar, 1993; Shock and Koretsky, 1995; Sverjensky et al., 1997, 2014; Schulte et al., 2001). Recently the HKF model was extended to 6.0 GPa and 1200 °C via molecular-dynamic estimates of the dielectric constant of water (Pan et al., 2013; Sverjensky et al., 2014). These new pressure and temperature limits inspired the design of a nuclear magnetic resonance (NMR) probe for examining solute speciation at higher pressures (Pautler et al., 2014; Ochoa et al., 2015).

There is a rich literature on high-pressure NMR spectroscopy, but this earlier work is generally limited to pressures less than 0.5 GPa (see Ballard et al., 1996), with heroic exceptions (Jonas, 1980; Lang and Lüdemann,

1993; de Langen and Prins, 1995; Ballard et al., 1998). These earlier designs generally employed milliliter-sized samples. In contrast, the design described in the present paper has a 10–15 microliter sample volume (Fig. 1) and can reach pressures of 2.0 GPa. The early work was directed at detailing solvent motions and relaxation mechanisms (Lee and Jonas, 1971; Lee et al., 1974; Akai and Jonas, 1976; Jonas et al., 1976; Defries and Jonas, 1977; Jonas, 1980; Lamb et al., 1981; Lamb and Jonas, 1981; Lang and Lüdemann, 1993; Ballard et al., 1998). High-pressure NMR was then extended to estimate the activation volumes of homoleptic reactions (Merbach and Vanni, 1977; Asano and Noble, 1978; Ducommun et al., 1979a,b, 1980; Monnerat et al., 1981; Swaddle and Merbach, 1981; Meyer et al., 1982; Hugi-Cleary et al., 1985, 1987; Cossy et al., 1987; Minirale, 1989; Pittet et al., 1990; Takagi et al., 1994; Drljaca et al., 1998a; Swaddle et al., 2005; Dees et al., 2007) with an intent of assigning mechanisms to ligand-exchange reactions (Helm and Merbach, 2005). The work has been reviewed several times (Asano and Noble, 1978; Eldik et al., 1989; Drljaca et al., 1998b). Diamond-anvil technologies, of course, can reach much higher pressures but are limited to nanoliter sample volumes or less, which are too small for studying solutes in water (e.g., Meier et al., 2015).

In this paper, the NMR spectroscopy of a fully dissociated electrolyte (CsCl, LaCl$_3$) is studied in order to reproduce the earlier work of Lee et al. (1974) and to demonstrate the utility of the new probe design. Time constants for the longitudinal relaxation (T_1) of ^{2}H were measured on aqueous CsCl in D$_2$O and compare well with the original work. In addition, values of T_1 were determined for ^{133}Cs and ^{2}H NMR in the solutions and were compared to previous work on LaCl$_3$ (Lee and Jonas, 1971; Lee et al., 1974; Ochoa et al., 2015). The CsCl and LaCl$_3$ solutions were chosen because Jonas' group not only measured the T_1 values for these solu-

tions, but also measured viscosities via the rolling-ball method at high pressures. Knowing the viscosity of an experimental solution is important because this controls rates of molecular tumbling and thus affects the widths of NMR spectral peaks.

2. EXPERIMENTAL METHODS

All cesium chloride (CsCl) solutions were prepared by dissolving the anhydrous salt into deuterium oxide solvent (D$_2$O). Lanthanum chloride (LaCl$_3$) solutions were made similarly but in H$_2$O with a resistance of 18 MΩ. Solution compositions were verified by coulometric titration for the chloride ion. All pD and pH measurements were made with a combination electrode and calibrated using standard buffers in H$_2$O. The pD values were calculated using: pD = pH + 0.4 (Kręzel and Bal, 2004).

The design of the high-pressure NMR probe is described in earlier papers (Pautler et al., 2014; Ochoa et al., 2015) and only the highlights are mentioned here. This high-pressure NMR probe is distinct from previous designs (e.g., Ballard et al., 1996, 1998) because it employs a small solenoid coil made of Berylco-25 wire wrapped around cylindrical capsule of PEEK© (Polyether ether ketone) tubing containing 10–15 μL experimental solution. The cylindrical capsule is sealed at each end (Fig. 1.A) with waterproof epoxy. The solenoid is fabricated from 28 gauge beryllium-copper wire and fed through small holes in the assembly where it is sealed with Stycast© epoxy mixed with a small amount of Al$_2$O$_3$ powder (Fig. 1.B). A ruby attached to a 200 μm fiber-optic cable is also passed through the feedthrough, just below the RF coil, and sealed. Pressure was monitored *in situ* using ruby fluorescence where movement of the R1 peak with pressure (Piermarini et al., 1975; Mao et al., 1986) could be monitored using an Ocean Optics HR4000 UV–vis spectrometer. To ensure that the lowest-pressure measurements were accurate, we confirmed the ruby-fluorescence calibration via a four-wire resistance measurement on manganin wire (Supplemental Information). The correlation is nearly exact (Supplemental Information) but we use the fluorescence estimates of pressure throughout this paper because they can be made *in situ*.

The ^{133}Cs and ^{2}H NMR data were acquired using a 300 MHz (7.0 T) Oxford Instruments 78-mm-bore superconducting magnet interfaced to a spectrometer controlled by Tecmag Orion® software. The ^{2}H T_1 measurements were acquired using a standard inversion-recovery pulse sequence with a calibrated π/2 time of 15.8 μs and a relaxation delay of 3 s (applied peak-to-peak radiofrequency voltage of 130 V with a circuit Q ∼ 11). The ^{133}Cs T_1 measurements were acquired using a saturation-recovery pulse sequence with a calibrated π/2 of 9 μs and a relaxation delay of 100 ms. The probe includes a cooling jacket through which water was circulated at 25($\pm$2) °C from an external water bath. The two degree range corresponded to a diurnal variation. Temperature in the probe was checked with a Type T thermocouple. The experimental range in temperature during an experiment was much smaller at 25 °C ($\pm$0.5 °C).
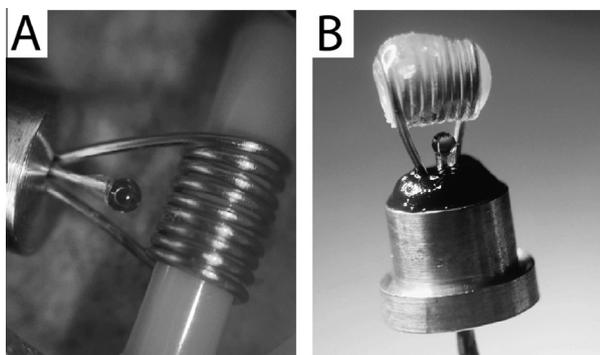

Fig. 1. The microcoil geometry, showing the 1-mm-diameter ruby sphere that is attached to a fiberoptic cable for pressure measurements and calibration. (A): Solenoid and ruby before a solution sample has been placed in the 10–15 μL PEEK© tubing container, and before trimming, with no Stycast© added to seal the beryllium-copper feedthrough. The coil length is 3.4 mm and the coil diameter is 2.7 mm. (B): The solenoid ready for an experiment. The sample is sealed into the tubing and the assembly is sealed with Stycast© mixed with Al$_2$O$_3$ powder.

The self-diffusion coefficients of H_2O in aqueous solutions were measured using ^1H NMR on a permanent-magnet-based Aspect Imaging MR-100 instrument at 43.7 MHz (1.0 T) that is interfaced to a Tecmag Apollo Spectrometer. A standard pulsed-gradient spin-echo (PGSE) pulse sequence was used with a field-gradient pulse length of $\delta = 10$ ms and a gradient-pulse spacing of $\Delta = 100$ ms (Stilbs, 1987; Antalek, 2002). The $\pi/2$ pulse time was calibrated to 15 μs for all solutions. Parameters were extracted from the measured data with a Matlab code by fitting the signal intensity to an exponential decay (Stejskal and Tanner, 1965; Tanner and Stejskal, 1968). Temperature in the bore of this magnet was also monitored via a type-T thermocouple.

3. SOLUTION NMR

Rapid tumbling of small molecules in a strong magnetic field causes the longitudinal and transverse relaxation times to become equivalent ($T_1 = T_2$). In this "extreme narrowing" limit, the longitudinal relaxation rates of quadrupolar nuclei ($I > \emptyset$), such as ^2H and ^{133}Cs can be determined from (Harris, 1986):

$$\frac{1}{T_{1Q}} = \frac{1}{T_{2Q}} = \frac{3}{10}\pi^2 \frac{2I+3}{I^2(2I-1)}\langle\chi^2\rangle\tau_c \qquad (1)$$

where I is the spin of the nucleus, τ_c is the reorientation time of the molecule, and $\langle\chi^2\rangle$ is the mean square of the zero-average quadrupolar-coupling constant.

The reorientation time of the molecule, τ_c, depends upon solution viscosity and can be described using the Stokes–Einstein equation as:

$$\tau_c = \frac{\eta\kappa V_m}{kT} \qquad (2)$$

where η is macroscopic viscosity, V_m is hydrodynamic volume, and κ is a theoretical constant that describes the ratio of intermolecular torques on the solute molecule to the intermolecular forces of the solvent molecules (McClung and Kivelson, 1968; Kivelson et al., 1970). The value for κ is typically set to unity, so that V_m can be treated as the effective hydrodynamic volume. In these experiments, that volume would be D_2O, H_2O, or a single Cs^+ or La^{3+} ion in solution.

The solution viscosity increases with pressure, which originally motivated (Lee et al., 1974) to directly measure viscosity in the high-pressure solutions. Here estimates in the pressure-variation of viscosity can be determined via measurements of the diffusion coefficient of H_2O using the alternative expression:

$$D = \frac{kT}{6\pi\eta r} \qquad (3)$$

where D is the self-diffusion coefficient of molecules in the solvent, r is the hydrodynamic radius of the molecule and all other variables retain their usual definitions (Edward, 1970). In evaluating Eq. (3), a hydrodynamic radius for water of 1.379 Å is used (Woessner, 1964; Rahman and Stillinger, 1971) and assumed to be independent of pressure.

The diffusion coefficient of H_2O was measured via a variation of a method employed by Akai and Jonas (1976) that is well developed for ambient pressure (Stejskal and Tanner, 1965; Tanner and Stejskal, 1968). In the PGSE experiment, the apparent signal-decay time constant is measured with a spin-echo experiment as function of the strength of the applied magnetic-field gradient pulses. The Akai and Jonas (1976) method employed a static gradient. For the work reported here, the PGSE pulse sequence is a standard $\pi/2$-pulse followed by a π-pulse. Following the first $\pi/2$-pulse, an initial magnetic-field gradient pulse is applied with length δ. Subsequently, at a time Δ later than the initial gradient, a second gradient pulse with an identical length δ is applied. The apparent diffusion coefficient is determined by fitting the measured intensity data to the following equation (Stejskal and Tanner, 1965; Tanner and Stejskal, 1968):

$$S = S_0 \exp\left[-\gamma^2 G^2 \delta^2 \left(\Delta - \frac{\delta}{3}\right)D\right] \qquad (4)$$

where S_o is signal intensity in the absence of a gradient, γ is the gyromagnetic ratio, G is the strength of the gradient pulse in Tesla/m, and D is the apparent diffusion coefficient. During the field gradient pulse, the signal intensity, S, decreases exponentially as a function of time and as a function of G. These intensity data are then fit to Eq. (4) in order to calculate D, the apparent diffusion coefficient, with uncertainties established as the precision of four trials. This value is 'apparent' because the actual magnetic-field gradients affecting the microcoil sample are not known with certainty, only the field gradients produced by the spectrometer. Conventionally, such geometry-specific effects are eliminated by using a well-accepted standard to scale the measurements. An accepted value for the diffusion coefficient of H_2O at 20 °C is 2.025×10^{-9} m^2/s (Holz et al., 2000). This value is used to scale the apparent measurements, which are within a factor of two of this number at ambient pressures. An assumption is made that the scaling does not vary with pressure, which is reasonable since controls of the magnetic-field gradients are exterior to the probe. The coil and sample are also not considerably deformed by the hydrostatic pressure.

4. RESULTS

4.1. ^2H and ^{133}Cs NMR relaxation rates in CsCl solutions compared to LaCl$_3$ solutions

The T_1 values for ^2H in various solutions at 25 °C are shown in Fig. 2.A. The values for pure D_2O at 25 °C (this paper) and at 10 °C and 30 °C from Jonas' group (Lee et al., 1974) are shown in Fig. 2.B. The results using the microcoil probe are bracketed by the previous work at near temperatures (Fig. 2.B). The similarity between the T_1 values reported here and those reported previously indicates that the microcoil sample is not being heated by repeated pulsing and that the NMR probe design is trustworthy. The maximum in T_1 values with pressure has generally been interpreted to indicate pressure-enhanced structuring of the solvent. The microcoil design has much less precise control
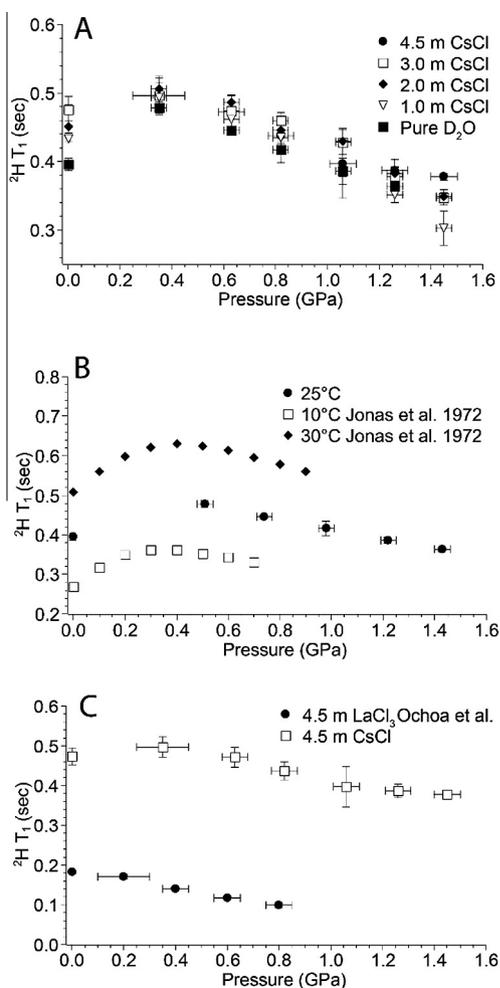
Fig. 3. T_1 values for ^{133}Cs for various CsCl solutions in D_2O at 25 (±0.5) °C. Errors assigned to pressure (±30 MPa) for 1.0 m, 2.0 m, and 3.0 m solutions, were determined by propagating a ±0.01 nm estimated uncertainty in the R1 fluorescence peak position through the equations relating the ruby fluorescence shift to pressure (Dewaele et al., 2008). Uncertainties for the 4.5 m CsCl solution (±100 MPa) were determined using a standard curve relating hydraulic press force to pressure measured in separate samples from ruby fluorescence (Ochoa et al., 2015). Uncertainties in the T_1 values correspond to a single estimated standard deviation of triplicate measurements.

Fig. 2. (A): ^2H T_1 values as a function of pressure for various solutions at 25(±0.5) °C. (B): ^2H T_1 data values as a function of pressure for pure D_2O compared with previous data (Lee and Jonas, 1972). (C): Values of ^2H T_1 for CsCl and $LaCl_3$ solutions (Ochoa et al., 2015) at 25(±0.5) °C. Errors assigned to pressure (±30 MPa) was determined by propagating a ±0.01 nm estimated uncertainty in the R1 fluorescence peak position through the equations relating the ruby fluorescence shift to pressure (Dewaele et al., 2008). Uncertainties in the T_1 values correspond to the estimated standard deviation of triplicate measurements.

over pressure at $P < 0.4$ GPa than the large-volume design of Lee et al. (1974), but it can recapture the characteristic maxima in ^2H T_1 values observed for all CsCl solutions. Lee et al. (1974) report the maximum at about 0.3–0.5 GPa. Comparison of ^2H T_1 values in a 4.5 m CsCl and $LaCl_3$ solutions indicate that the steady decline in T_1 values with pressure is similar (Fig. 2.C). Beyond the 0.5 GPa maxima, the T_1 values for all D_2O solutions decrease uniformly (Fig. 2) and this decrease has been interpreted as resulting from an increase in solution viscosity (Lee et al., 1974).

The ^{133}Cs T_1 values of CsCl solutions (Fig. 3) also decrease uniformly with pressure and the rate of decrease is nearly, but not completely, independent of solution composition. These results contrast with previous work on
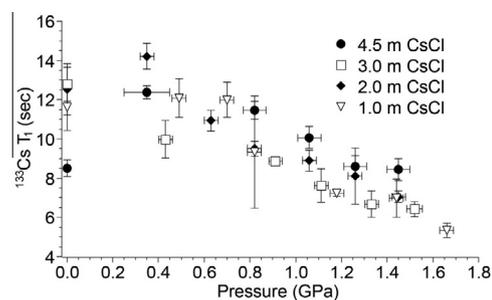
LaCl$_3$ solutions where the ^{139}La T_1 values vary considerably with electrolyte concentrations at ambient pressures (Ochoa et al., 2015). For example, at ambient pressures, an increase of $LaCl_3$ concentration from 1.0 m to 4.5 m is accompanied by a large decrease in the T_1 values from 1.11(±0.02) ms to 0.18(±0.09) ms (Ochoa et al., 2015). In contrast, T_1 values for ^{133}Cs decrease only from 11.6 (±1.2) s to 8.5(±0.4) s over a similar range in concentration. The difference is also manifested in the properties of the solvent. For example, the T_1 values for ^2H in 1.0 m and 4.5 m $LaCl_3$ are 0.27(±0.02) and 0.18(±0.005) s, respectively. This difference is much larger than in similar CsCl solutions, where the ^2H T_1 values are 0.43(±0.04) s and 0.47(±0.02) s for 1.0 m and 4.5 m CsCl solutions, respectively.

4.2. Diffusion coefficients for H_2O at pressure

As was originally concluded by the Jonas group, pressure variations in T_1 values reflect changes in viscosity of the solution. As described above, the viscosity can be estimated from measurement of an apparent diffusion coefficient using the PGSE pulse sequence. The apparent diffusion coefficients for H_2O in both pure water and in a 1.0 m CsCl solution measured here are shown in Fig. 4.A. Note that the D values for both solutions decrease uniformly with pressure and that these trends match well the pressure variation of T_1 values shown in Figs. 2 and 3. Solutions viscosities were calculated via Eq. (3) and are reported in Table 1.

If changes in viscosity alone caused the measured variation in T_1 values with pressure, then the ratio of D/T_1 would be independent of pressure. Such a ratio is shown as Fig. 4.B. As one can see, the ratios for all conditions lie within 10 % of each other and are independent of pressure, within experimental error.
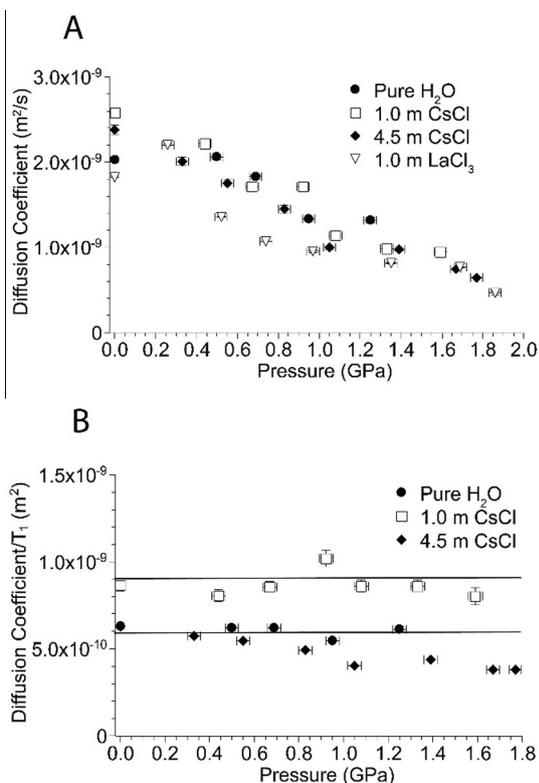
Fig. 4. (A): Self-diffusion coefficients for H_2O in water and aqueous solutions of 1.0 m CsCl, 4.5 m CsCl, or 1.0 LaCl$_3$ at 20 ($\pm$0.5) °C. (B): The diffusion coefficients divided by the ^1H T_1 measurements for pure H_2O and for aqueous 1.0 m CsCl. Uncertainties from pressure were determined by propagating a $\pm$0.01 nm ($\pm$30 MPa) estimated uncertainty in the peak position through the equations relating the R1 fluorescence of the ruby to pressure (Dewaele et al., 2008). Error estimates assigned to diffusion coefficient values are the estimated standard deviation from four repeated PGSE trials. The lines are merely to guide the eye and are not regressions.

4.3. Evidence for suppressed freezing

Pressure was applied to all CsCl solutions until they froze, which was inferred from the disappearance of the ^{133}Cs NMR peak, or when the ^2H linewidth increased beyond the bandwidth of the detector. When pressure was subsequently relieved in order to return the sample to ambient conditions, the NMR spectra were reacquired and yielded the T_1 value expected for the homogeneous solution, as one would expect for reversible freezing. The estimated pressures when each solution froze are reported in Fig. 5, with respect to various phase boundaries. Ice-V and Ice-VI phase boundaries were reproduced from the results of Wagner et al. (1994). The phase boundary for metastable ice was reproduced from Whittaker et al. (1998) and is labeled in the figure as 'new ice'. Lines in Fig. 5 also identify the solid–liquid phase boundary in the presence of different NaCl concentrations in H_2O (Journaux et al., 2013). As one can see, the experimental freezing points exceed by almost a factor of two the pressures expected from the phase boundary between liquid

Table 1
Diffusion coefficients and calculated viscosities for pure water and for 1.0 m CsCl solution at 20($\pm$0.5) °C. Diffusion coefficients in this table are estimated by dividing the measured value at ambient pressure by an accepted diffusion coefficient value for water at 20 °C of 2.025×10^{-9} m^2/s (Holz et al., 2000). Uncertainties are reported as an estimated standard deviation. Uncertainties in the pressure estimates are $\pm$0.03 GPa.

Pressure (GPa)	Diffusion (m^2/s)	Viscosity (cP)
Pure H$_2$O		
1.01×10^{-4}	$2.03 \times 10^{-9} \pm 2.8 \times 10^{-11}$	0.77 ± 0.01
0.50	$2.06 \times 10^{-9} \pm 2.8 \times 10^{-11}$	0.75 ± 0.01
0.69	$1.83 \times 10^{-9} \pm 2.05 \times 10^{-11}$	0.85 ± 0.01
0.95	$1.33 \times 10^{-9} \pm 1.1 \times 10^{-11}$	1.17 ± 0.01
1.25	$1.32 \times 10^{-9} \pm 3.0 \times 10^{-11}$	1.18 ± 0.03
1.0 m CsCl in H$_2$O		
1.01×10^{-4}	$2.58 \times 10^{-9} \pm 2.3 \times 10^{-11}$	0.60 ± 0.005
0.44	$2.22 \times 10^{-9} \pm 2.6 \times 10^{-11}$	0.70 ± 0.01
0.67	$1.71 \times 10^{-9} \pm 1.9 \times 10^{-11}$	0.91 ± 0.01
0.92	$1.71 \times 10^{-9} \pm 1.6 \times 10^{-11}$	0.91 ± 0.01
1.08	$1.14 \times 10^{-9} \pm 1.1 \times 10^{-11}$	1.37 ± 0.01
1.33	$9.87 \times 10^{-10} \pm 9.9 \times 10^{-12}$	1.58 ± 0.03
1.59	$9.49 \times 10^{-10} \pm 1.4 \times 10^{-11}$	1.64 ± 0.02
4.5 m CsCl in H$_2$O		
1.01×10^{-4}	$2.38 \times 10^{-9} \pm 5.1 \times 10^{-11}$	0.65 ± 0.01
0.33	$2.01 \times 10^{-9} \pm 4.8 \times 10^{-11}$	0.78 ± 0.02
0.55	$1.75 \times 10^{-9} \pm 4.8 \times 10^{-11}$	0.89 ± 0.02
0.83	$1.45 \times 10^{-9} \pm 4.8 \times 10^{-11}$	1.07 ± 0.04
1.05	$9.99 \times 10^{-10} \pm 1.95 \times 10^{-11}$	1.56 ± 0.03
1.39	$9.79 \times 10^{-10} \pm 1.95 \times 10^{-11}$	1.59 ± 0.03
1.67	$7.44 \times 10^{-10} \pm 1.5 \times 10^{-11}$	2.09 ± 0.04
1.77	$6.47 \times 10^{-10} \pm 1.1 \times 10^{-11}$	2.40 ± 0.04
1.0 m LaCl$_3$ in H$_2$O		
1.01×10^{-4}	$1.83 \times 10^{-9} \pm 5.2 \times 10^{-12}$	0.85 ± 0.01
0.26	$2.20 \times 10^{-9} \pm 1.4 \times 10^{-11}$	0.71 ± 0.01
0.52	$1.36 \times 10^{-9} \pm 5.1 \times 10^{-12}$	1.15 ± 0.01
0.74	$1.07 \times 10^{-9} \pm 2.1 \times 10^{-12}$	1.45 ± 0.01
0.97	$9.57 \times 10^{-10} \pm 8.2 \times 10^{-12}$	1.63 ± 0.01
1.35	$8.14 \times 10^{-10} \pm 1.0 \times 10^{-11}$	1.91 ± 0.02
1.69	$7.66 \times 10^{-10} \pm 4.2 \times 10^{-12}$	2.03 ± 0.01
1.86	$4.67 \times 10^{-10} \pm 1.8 \times 10^{-11}$	3.34 ± 0.13

water and Ice VI of $\sim$0.9 GPa. The points plotted on Fig. 5, however, correspond to a crude estimate of the actual freezing pressure – we cannot identify frozen samples in our NMR probe. We can only report the last pressure where the NMR spectra exhibited liquid-like behavior, where the T_1 values, for example, could be measured, and the jumps in pressure were sufficiently large that the plotted data do not indicate phase boundaries.

5. DISCUSSION

5.1. Relaxation in fully dissociated electrolytes

The differences in T_1 relaxation values at ambient conditions for solutions of various CsCl and LaCl$_3$ concentrations are expected since these electrolytes affect the structure of water differently. Electrolytes are classified as 'structure-breaking' or 'structure-making' according to their effects on NMR relaxation and the structure of water
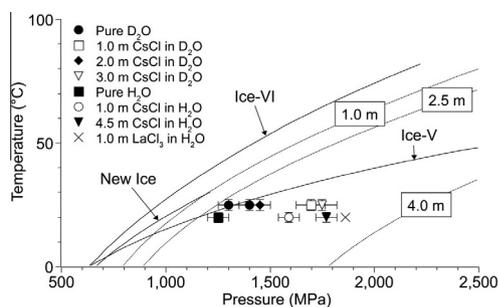
Fig. 5. Estimated minimum freezing pressures of the experimental solutions relative to various phase boundaries for water. These pressures are inferred from the disappearance of liquid-like NMR behavior. Curves for Ice-V and Ice-VI were constructed from Wagner et al. (1994). The curve for metastable ice, labeled 'New Ice' was reproduced from Whittaker et al. (1998). The curves describing the salt-effected freezing of NaCl solutions are shown as various lines labeled: '4.0 m', '2.5 m' and '1.0 m' (from Journaux et al., 2013). A sample of 1.0 m LaCl$_3$ showed liquid-like NMR spectra all the way to 1.86 GPa and the final pressure is shown as an '×'.

(Cox and Wolfenden, 1934; Hribar et al., 2002; Marcus, 2009). Structure-breaking ions, like Cs$^+$, allow solvent molecules to rotate more freely when added to pure water and structure-making ions, like La^{3+}, restrict the rotation of solvent molecules by binding tightly to the bulk solvent lattice. Thus, addition of CsCl or LaCl$_3$ salts to water has a different effect on the T_1 values of ^{133}Cs, ^{139}La and ^{2}H. Although LaCl$_3$ solutions exhibit a range of ^{139}La T_1 values for different electrolyte concentrations at ambient conditions, the ^{139}La T_1 values decrease and become nearly equal for different LaCl$_3$ concentrations at $P > 1.5$ GPa (Ochoa et al., 2015). Pressure eliminates the differences in T_1 values for different solutions.

5.2. Viscosity of aqueous solutions at pressure and NMR spectroscopy

The decrease in ^{2}H and ^{133}Cs T_1 values to 1.7 GPa are largely attributable to increases in viscosity, leading to corresponding increases in the reorientation times and shorter T_1 values. This result is important. The broadening with

pressure of these signals can, under ideal circumstances, be interpreted to indicate pressure-induced changes in reaction rates and thus activation volumes. Although high-pressure NMR studies of reaction kinetics are usually over a narrow range of pressure (0.1–0.35 GPa) where viscosity-caused line broadening may be minimal, the contribution of viscosity will be increasingly important as high pressures are reached. As one can see in Tables 1 and 2, the increases in solution viscosities with pressure are monotonic and can probably be predicted from a simple regression. This agreement is important because the data in Table 2 were measured by Jonas' group using a completely different method. They employed a rolling sphere to estimate the viscosity from optical measurements. Our data using the NMR method not only compare well with these independent methods, but also show approximately the same variation with pressure.

5.3. Suppressed freezing and metastability

There are two causes of the apparent overpressurization of these solutions. First, the NaCl electrolyte concentration has been shown by Journaux et al. (2013) to suppress the freezing of H$_2$O at pressure. Although our electrolyte is CsCl in D$_2$O and not NaCl in H$_2$O, it is reasonable to expect a similar suppression of the freezing point in a Raoult's Law sense. The differences between the freezing point of pure D$_2$O and H$_2$O at high pressures are very small (Brown and Whalley, 1966; Pistorius et al., 1968).

Secondly, freezing is slow in these experiments. An example is shown in Fig. 6 for the 3.0 m CsCl solution. The figure demonstrates solution freezing at 1.75 GPa after 15 min, as gauged by the slow disappearance of the NMR signal. As mentioned above, temperature estimates seem to be accurate and indicate that the sample is not heated by the radio frequency pulse in the saturation-recovery pulse sequence. Similarly, there is no evidence for a pressure gradient, such as would be established if the pressure medium froze (Koyama-Nakazawa et al., 2007). Similar over-pressurization of the samples is observed when either fluorocarbon liquid or Daphne 7373 oil is used as the pressure medium. Both of these liquids are expected to remain liquid at these conditions. The simplest explanation for the relatively high freezing pressures is that higher pressures

Table 2
Viscosity measurements via the rolling-ball method as a function of pressure for pure H$_2$O and 4.5 m CsCl in D$_2$O at 10 °C and 30 °C (Jonas et al., 1976). Note that these values are about the same size as those reported in Table 1 that were measured independently via NMR methods, and that the change is similar with pressure.

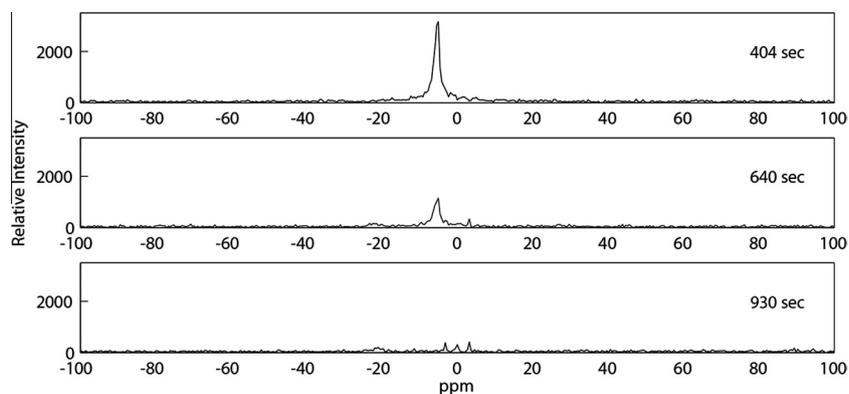| Pressure (GPa)	Viscosity (cP) pure H$_2$O at 10 °C	Viscosity (cP) pure H$_2$O at 30 °C	Viscosity (cP) 4.5 m CsCl in D$_2$O at 30 °C
1.013×10^{-4}	1.31	0.801	0.966
0.1	1.26	0.811	1.001
0.2	1.29	0.846	1.059
0.3	1.37	0.899	1.156
0.4	1.47	0.963	1.252
0.5	1.60	1.04	
0.6	1.76	1.13	
0.7	1.94	1.23	
0.8		1.34	
0.9		1.45	

Fig. 6. Sequential ^{133}Cs NMR spectra for 3.0 m CsCl at 1.75 GPa. The signal loss after 930 s indicates freezing. The remaining small peaks seen at 930 s are noise.

can be reached via the combined effects of freezing-point depression by the electrolyte and solution metastability.

6. CONCLUSIONS AND IMPLICATIONS FOR GEOCHEMISTRY

There are several important geochemical results from this study. Foremost is that the NMR probe design allows measurements on solutions to 2.0 GPa. The T_1 relaxation times for ^{2}H, ^{133}Cs, and ^{139}La in CsCl, LaCl$_3$, and pure D$_2$O solutions are reproducible and match well with the earlier work at similar pressures, indicating that the probe is effective. Although this study only deals with fully dissociated electrolytes, the probe can resolve signals from various aqueous complexes (Pautler et al., 2014), yielding equilibrium constants and kinetic information about chemical reaction rates. Thermodynamic data about speciation is codified as reaction volumes and compressibilities (Asano and Noble, 1978; Eldik et al., 1989; Drljaca et al., 1998a), and pressure is particularly useful for understanding the role of solvation or changes in coordination in aqueous reactions (Helm and Merbach, 2005; Swaddle et al., 2005), including isomerization of large molecules (e.g., Johnson et al., 2013).

There is a rich chemistry to explore. As mentioned in the *Introduction*, the range of geochemical models for solution thermodynamics was recently extended via molecular-dynamic estimates of the dielectric properties of water to 6.0 GPa and 1200 °C (Pan et al., 2013; Sverjensky et al., 2014). The advance allowed Sverjensky and Huang (2015) to discover a pH-driven pathway for forming diamonds at 5.0 GPa. These pressures, however, are well beyond the current capabilities of conventional hydrothermal solution spectroscopies, yet through judicious choice of nonmagnetic, high-strength alloys (e.g., Uwatoko et al., 2002), it should not be difficult to extend the 2.0 GPa pressure range of the probe described above to 3.5–4.0 GPa.

The influence of electrolytes on freezing has obvious implications for the transport of liquid water to depths in the Earth, or in salty exoplanets, a point understood by Journaux et al. (2013). Although the freezing points of CsCl and LaCl$_3$ aqueous solutions have not yet been evaluated as a function of pressure, it is reasonable to expect a similar

effect to that which is found for NaCl solutions (Journaux et al., 2013). Furthermore, and most interestingly, the crystallization of high-pressure ices from these solutions at pressure is sufficiently slow that NMR spectra can be acquired. We, of course, know nothing of the phases that precipitate when we lose liquid-like NMR signals from these solutions, but these questions await further experimentation.

Finally, transport properties of molecules can be measured easily at pressure, such as the diffusion coefficients shown in Fig. 5. These estimates were previously possible but extraordinarily difficult since the velocities of rolling spheres must be measured at pressure (Abramson, 2007). Yet knowing the viscosity of the solution is essential for using NMR information to infer reaction rates. The activation volumes for the interconversion reactions are often inferred from broadening of the NMR signals as a function of pressure (e.g., Johnson et al., 2013). At the high pressures of this study, contributions to the NMR linewidth from increased solvent viscosity are appreciable, but can be estimated directly and easily (Fig. 5).

APPENDIX A. SUPPLEMENTARY DATA

Supplementary data associated with this article can be found, in the online version, at http://dx.doi.org/10.1016/j.gca.2016.08.013.

REFERENCES

Abramson E. H. (2007) Viscosity of water measured to pressures of 6 GPa and temperatures of 300 °C. *Phys. Rev. E* **76**, 051203.

Akai J. A. and Jonas J. (1976) The effect of pressure and temperature on self-diffusion coefficients in several concentrated deuterium oxide diamagnetic electrolyte solutions. *J. Solution Chem.* **5**, 563–574.

Anderson M. and Crerar D. A. (1993) *Thermodynamics in Geochemistry: The Equilibrium Model*. Oxford, pp. 453–463.

Antalek B. (2002) Using pulsed gradient spin echo NMR for chemical mixture analysis: how to obtain optimum results. *Concepts Magn. Reson.* **14**, 225–258.

Asano T. and Noble W. J. L. E. (1978) Activation and reaction volumes in solution. *Chem. Rev.* **78**, 407–489.

Ballard L., Reiner C. and Jonas J. (1996) High-resolution NMR probe for experiments at high pressures. *J. Magn. Reson., Ser. A* **123**, 81–86.

Ballard L., Yu A., Reiner C. and Jonas J. (1998) A high-pressure, high-resolution NMR probe for experiments at 500 MHz. *J. Magn. Reson.* **133**, 190–193.

Brown A. J. and Whalley E. (1966) Preliminary investigation of the phase boundaries between ice VI and VII and ice VI and VIII. *J. Chem. Phys.* **45**, 4360–4361.

Cossy C., Helm L. and Merbach A. E. (1987) 138. Dimethylformamide-exchange mechanism on some first-row divalent transition-metal ions. *Helv. Chim. Acta* **70**, 1516–1525.

Cox W. M. and Wolfenden J. H. (1934) The viscosity of strong electrolytes measured by a differential method. *Proc. R. Soc. Lond. Ser. A* **145**, 475–488.

de Langen M. and Prins K. O. (1995) NMR probe for high pressure and high temperature. *Rev. Sci. Instrum.* **66**, 5218–5221.

Dees A., Zahl A., Puchta R., Hommes N. J. R. V. E., Heinemann F. W. and Ivanovic-Burmazovic I. (2007) Water exchange on seven-coordinate Mn(II) complexes with macrocyclic pentadentate ligands: insight in the mechanism of Mn(II) SOD mimetics. *Inorg. Chem.* **46**, 2459–2470.

Defries T. and Jonas J. (1977) Molecular motions in compressed liquid heavy water at low temperatures. *J. Chem. Phys.* **66**, 5393–5399.

Dewaele A., Torrent M., Loubeyre P. and Mezouar M. (2008) Compression curves of transition metals in the Mbar range: experiments and projector augmented-wave calculations. *Phys. Rev. B* **78**, 1–13.

Drljaca A., Zahl A. and Van Eldik R. (1998a) High-pressure oxygen-17 NMR study of the dihydroxo-bridged rhodium (III) hydrolytic dimer. Mechanistic evidence for limiting dissociative water exchange pathways. *Inorg. Chem.* **37**, 3948–3953.

Drljaca C., Hubbard C. D., Eldik R., Van Asano. T., Basilevsky M. V. and LE Noble W. J. (1998b) Activation and reaction volumes in solution. 3. *Chem. Rev.* **98**, 2167–2289.

Ducommun Y., Earl W. L. and Merbach A. E. (1979a) Oxygen-17 FT NMR study of the effect of pressure on the exchange of water on nickel(II). *Inorg. Chem.* **18**, 2754–2758.

Ducommun Y., Newman K. E. and Merbach A. E. (1979b) High pressure ^{17}O-FT-NMR. Evidence for the associative nature of substitution reactions on Mn^{2+} in water. *Helv. Chim. Acta* **62**, 2511–2516.

Ducommun Y., Newman K. E. and Merbach A. E. (1980) High-Pressure ^{17}O NMR evidence for a gradual mechanistic change-over from Ia to Id for water exchange on divalent octahedral metal ions going from manganese(II) to nickel(II). *Inorg. Chem.* **19**, 3696–3703.

Edward J. T. (1970) Molecular volumes and the Stokes-Einstein equation. *J. Chem. Educ.* **47**, 261–270.

Van Eldik R., Asano T. and Noble W. J. L. (1989) Activation and reaction volumes in solution. 2. *Chem. Rev.* **89**, 549–688.

Harris R. K. (1986) *Nuclear Magnetic Resonance Spectroscopy*. Longman Scientific & Technical, New York, pp. 85–88.

Helm L. and Merbach A. E. (2005) Inorganic and bioinorganic solvent exchange mechanisms. *Chem. Rev.* **105**, 1923–1959.

Holz M., Heil S. R. and Sacco A. (2000) Temperature-dependent self-diffusion coefficients of water and six selected molecular liquids for calibration in accurate ^{1}H NMR PFG measurements. *Phys. Chem. Chem. Phys.* **2**, 4740–4742.

Hribar B., Southall N. T., Vlachy V. and Dill K. A. (2002) How ions affect the structure of water. *J. Am. Chem. Soc.* **124**, 12302–12311.

Hugi-Cleary D., Helm L. and Merbach A. E. (1985) Variable-temperature and variable-pressure ^{17}O-NMR study of water exchange of hexaaquaaluminium(III). *Helv. Chim. Acta* **68**, 545–554.

Hugi-Cleary D., Helm L. and Merbach A. E. (1987) High pressure NMR kinetics. Part 30. Water exchange on hexaaquagallium (III): high-pressure evidence for a dissociative exchange mechanism. *J. Am. Chem. Soc.* **109**, 4444–4450.

Johnson R. L., Ohlin C. A., Pellegrini K., Burns P. C. and Casey W. H. (2013) Dynamics of a nanometer-size uranyl cluster in solution. *Angew. Chem.* **52**, 7464–7467.

Jonas J. (1980) Nuclear magnetic resonance studies at high pressures. *Rev. Phys. Chem. Japan* **50**, 19–35.

Jonas J., Defries T. and Wilbur D. J. (1976) Molecular motions in compressed liquid water. *J. Chem. Phys.* **65**, 582–588.

Journaux B., Daniel I., Caracas R., Montagnac G. and Cardon H. (2013) Influence of NaCl on ice VI and ice VII melting curves up to 6 GPa, implications for large icy moons. *Icarus* **226**, 355–363.

Kivelson D., Kivelson M. G. and Oppenheim I. (1970) Rotational relaxation in fluids. *J. Chem. Phys.* **52**, 1810–1821.

Koyama-nakazawa K., Koeda M., Hedo M. and Uwatoko Y. (2007) In situ pressure calibration for piston cylinder cells via ruby fluorescence with fiber optics. *Rev. Sci. Instrum.* **78**, 1–3.

Kręzel A. and Bal W. (2004) A formula for correlating pKa values determined in D_2O and H_2O. *J. Inorg. Biochem.* **98**, 161–166.

Lamb W. J. and Jonas J. (1981) NMR study of compressed supercritical water. *J. Chem. Phys.* **74**, 913–921.

Lamb W. J., Hoffman G. A. and Jonas J. (1981) Self-diffusion in compressed supercritical water. *J. Chem. Phys.* **74**, 6875–6880.

Lang E. W. and Lüdemann H. D. (1993) Density dependence of rotational and translational molecular dynamics in liquids studied by high pressure NMR. *Prog. Nucl. Magn. Reson. Spectrosc.* **25**, 507–633.

Lee Y. and Jonas J. (1971) Effect of pressure on proton spin-lattice relaxation in several concentrated aqueous electrolyte solutions. *J. Magn. Reson.* **5**, 267–272.

Lee Y. and Jonas J. (1972) Density effects on the dynamic structure of liquid deuterium oxide. *J. Chem. Phys.* **57**, 4233–4240.

Lee Y. K., Campbell J. H. and Jonas J. (1974) Effect of pressure on deuteron spin-lattice relaxation in several concentrated deuterium oxide diamagnetic electrolyte solutions. *J. Chem. Phys.* **60**, 3537–3543.

Mao H. K., Xu J. and Bell P. M. (1986) Calibration of the ruby pressure gauge to 800 kbar under quasi-hydrostatic conditions. *J. Geophys. Res.* **91**, 4673–4676.

Marcus Y. (2009) Effect of ions on the structure of water: structure making and breaking. *Chem. Rev.* **109**, 1346–1370.

McClung R. E. D. and Kivelson D. (1968) ESR linewidths in solution V studies of spin-rotational effects not described by rotational diffusion theory. *J. Chem. Phys.* **49**, 3380–3391.

Meier T., Reichardt S. and Haase J. (2015) High-sensitivity NMR beyond 200,000 atmospheres of pressure. *J. Magn. Reson.* **257**, 39–44.

Merbach A. E. and Vanni H. (1977) High-pressure, high-resolution nuclear magnetic resonance (HPHR-NMR): a tool in chemical kinetics. *Helv. Chim. Acta* **60**, 1124–1127.

Meyer F. K., Monnerat A. R., Newman K. E. and Merbach A. E. (1982) High-pressure NMR evidence for an associative

interchange mechanism, Ia, for solvent exchange on iron(III). *Inorg. Chem.* **21**, 774–778.

Minirale D. C. (1989) High-pressure NMR study. 38. Water-exchange mechanisms on the terbium to thulium octaaqualanthanide(III) ions: a variable-pressure oxygen-17 NMR study. *Inorg. Chem.* **28**, 2699–2703.

Monnerat A., Moore P., Newman K. E. and Merbach A. E. (1981) High pressure carbon-13 FT-NMR. Acetonitrile exchange with $[Co(CH_3CN)_6](ClO_4)_2$. *Inorganica Chim. Acta* **47**, 139–145.

Ochoa G., Pilgrim C. D., Martin M. N., Colla C. A., Klavins P., Augustine M. P. and Casey W. H. (2015) ^1H and ^{139}La NMR spectroscopy in aqueous solutions at geochemical pressures. *Angew. Chem. Int. Ed. Engl.* **127**, 15664–15667.

Pan D., Spanu L., Harrison B., Sverjensky D. A. and Galli G. (2013) Dielectric properties of water under extreme conditions and transport of carbonates in the deep Earth. *Proc. Natl. Acad. Sci.* **110**, 6646–6650.

Pautler B. G., Colla C. A., Johnson R. L., Klavins P., Harley S. J., Ohlin C. A., Sverjensky D. A., Walton J. H. and Casey W. H. (2014) A high-pressure NMR probe for aqueous geochemistry. *Angew. Chem. Int. Ed. Engl.* **53**, 9788–9791.

Piermarini G. J., Block S., Barnett J. D., Forman R. A., Piermarini G. J., Block S., Barnett J. D. and Forman R. A. (1975) Calibration of the pressure dependence of the R1 ruby fluorescence line to 195 kbar. *J. Appl. Phys.* **6**, 2774–2780.

Pistorius C. W. F. T., Rapoport E. and Clark J. B. (1968) Phase diagrams of H_2O and D_2O at high pressures. *J. Chem. Phys.* **48**, 5509–5514.

Pittet P.-A., Elbaze G., Helm L. and Merbach A. E. (1990) Tetrasolventoberyllium(II): high-pressure evidence for a sterically controlled solvent-exchange mechanism crossover. *Inorg. Chem.* **29**, 1936–1942.

Rahman A. and Stillinger F. H. (1971) Molecular dynamics study of liquid water. *J. Chem. Phys.* **55**, 3336–3359.

Schulte M. D., Shock E. L. and Wood R. H. (2001) The temperature dependence of the standard-state thermodynamic properties of aqueous nonelectrolytes. *Geochim. Cosmochim. Acta* **65**, 3919–3930.

Shock E. L. and Helgeson H. C. (1988) Calculation of the thermodynamic and transport properties of aqueous species at high pressures and temperatures: correlation algorithms for ionic species and equation of state predictions to 5 kb and 1000 °C. *Geochim. Cosmochim. Acta* **52**, 2009–2036.

Shock E. L. and Koretsky C. M. (1995) Metal-organic complexes in geochemical processes: estimation of standard partial molal thermodynamic properties of aqueous complexes between metal cations and monovalent organic acid ligands at high pressures and temperatures. *Geochim. Cosmochim. Acta* **59**, 1497–1532.

Shock E. L., Helgeson H. C. and Sverjensky D. A. (1989) Calculation of the thermodynamic and transport properties of aqueous species at high pressures and temperatures: standard partial molal properties of inorganic neutral species. *Geochim. Cosmochim. Acta* **53**, 2157–2183.

Stejskal E. O. and Tanner J. E. (1965) Spin diffusion measurements: spin echoes in the presence of a time-dependent field gradient. *J. Chem. Phys.* **42**, 288–292.

Stilbs P. (1987) Fourier transform pulsed-gradient spin-echo studies of molecular diffusion. *Prog. NMR Spectroscop.* **19**, 1–45.

Sverjensky D. A. and Huang F. (2015) Diamond formation due to a pH drop during fluid-rock interactions. *Nat. Commun.* **6**, 8702.

Sverjensky D. A., Shock E. L. and Helgeson H. C. (1997) Prediction of the thermodynamic properties of aqueous metal complexes to 1000 °C and 5 kb. *Geochim. Cosmochim. Acta* **61**, 1359–1412.

Sverjensky D. A., Harrison B. and Azzolini D. (2014) Water in the deep Earth: the dielectric constant and the solubilities of quartz and corundum to 60 kb and 1200 °C. *Geochim. Cosmochim. Acta* **129**, 125–145.

Swaddle T. W. and Merbach A. E. (1981) High-pressure oxygen-17 Fourier transform nuclear magnetic resonance spectroscopy. Mechanism of water exchange on iron(III) in acidic aqueous solution. *Inorg. Chem.* **20**, 4212–4216.

Swaddle T. W., Rosenqvist J., Yu P., Bylaska E., Phillips B. L. and Casey W. H. (2005) Kinetic evidence for five-coordination in $AlOH(aq)^{2+}$ Ion. *Science* **308**, 1450–1453.

Takagi H. D., Matsuda K., Aizawa S.-I., Funahashi S., Kinrade S. D. and Swaddle T. W. (1994) Variable-pressure dynamic NMR studies: effects of paramagnetic metal ions on NMR parameters in nonexchanging systems. *Can. J. Chem.* **72**, 2188–2192.

Tanger, IV, J. C. and Helgeson H. C. (1988) Calculation of the thermodynamic and transport properties of aqueous species at high pressures and temperatures: revised equations of state for the standard partial molal properties of ions and electrolytes. *Am. J. Sci.* **288**, 19–98.

Tanner J. E. and Stejskal E. O. (1968) Restricted self diffusion of protons in colloidal systems by the pulsed gradient, spin echo method. *J. Chem. Phys.* **49**, 1768–1777.

Uwatoko Y., Todo S., Ueda K., Uchida A., Kosaka M., Mori N. and Matsumoto T. (2002) Material properties of Ni–Cr–Al alloy and design of a 4 GPa class non-magnetic high-pressure cell. *J. Phys.: Condens. Matter* **14**, 11291–11296.

Wagner W., Saul A., Pruss A., Wagner W., Saul A. and Prup A. (1994) International equations for the pressure along the melting and along the sublimation curve of ordinary water substance. *J. Phys. Chem. Ref. Data* **23**, 516–527.

Whittaker R. H., Droser M. L., Bottjer D. J., Sheehan P. M., Chou I., Blank J. G., Goncharov A. F., Mao H. and Hemley R. J. (1998) In situ observations of a high-pressure phase of H_2O Ice. *Science* **281**, 809–813.

Woessner D. (1964) Molecular reorientation in liquids. Deuteron quadrupole relaxation in liquid deuterium oxide and perdeuterobenzene. *J. Chem. Phys.* **40**, 2341–2348.

Associate editor: Jeffrey G. Catalano